

# Application of SEBAL approach and MODIS time-series to map vegetation water use patterns in the data scarce Krishna river basin of India

Mobin-ud-Din Ahmad\*, Trent Biggs\*\*, Hugh Turrall\*, Christopher A. Scott\*\*

\* International Water Management Institute (IWMI), Global Research Division, PO Box 2075, Colombo, Sri Lanka. Tel: +94-11-2787404, Fax: +94-11-2786854, E-mail: a.mobin@cgiar.org (M.D. Ahmad); h.turrall@cgiar.org (H. Turrall)

\*\* International Water Management Institute (IWMI), Regional Office for South Asia c/o ICRISAT, Patancheru, AP 502 324, India, Tel: +91-40-3296161 Fax: 91-40-324-1239 E-mail: t.biggs@cgiar.org (T. Biggs); c.scott@cgiar.org (C.A. Scott)

## Abstract

Continually increasing world population requires additional food production in the face of growing water scarcity. Evapotranspiration from irrigated land, where much of the world's food is produced, is one of the most useful indicators to explain whether the water is used as "intended" or not. Remote sensing techniques have been developed and applied for the computation of actual evapotranspiration, mainly within irrigation systems. In this study a Landsat7 image of December 29, 2000 was acquired for a data scarce area with diverse land use in the Krishna Basin in India and actual evapotranspiration ( $ET_a$ ) was computed using the Surface Energy Balance Algorithm for Land (SEBAL). The image occurs approximately 2 months after the end of the monsoon rains, and between the major cropping cycles in the area. SEBAL  $ET_a$  varies between 0 to 4.7 mm per day over the image, which includes dense urban areas, dry/barren grassland, native vegetation including shrubs and deciduous forests, water bodies, rainfed crops, supplemental groundwater irrigated vegetables/cotton, groundwater/tank irrigated rice, and irrigated fodder grass/rice in the corridor downstream from the urban area where wastewater is used for irrigation. The estimated evaporation rate from permanent water bodies such as lakes is 4.7 mm per day, which is close to the measured pan evaporation rate of 4.8 mm per day. Irrigated fodder grass evaporates at a rate of 3.4-3.5 mm per day, almost the same as Penman-Monteith reference crop evapotranspiration of 3.5 mm per day computed using data from the nearby ICRISAT meteorological station.  $ET_a$  was quantified for different land use classes using polygons of representative land uses, including ground truth field work and visual interpretation of the image. Interpretation of MODIS imagery time series shows that the SEBAL  $ET_a$  values depends on crop phenology; the wastewater irrigated area has the highest  $ET_a$  in the image, partly due to its earlier cropping date compared with groundwater irrigated rice. Shrub and forests in the senescence phase have similar  $ET_a$  to vegetable/cash crops, and  $ET_a$  from grasslands falls rapidly to a low 0.8 mm per day following the end of the monsoon. The results indicate that wastewater irrigation of fodder and rice is sufficient to meet crop water demand; however, there appears to be deficit irrigation of rice using groundwater.

## Keywords

water management, irrigation, remote sensing, evapotranspiration, river basin, India

## INTRODUCTION

Judicious management of precious land and water resources will be one of the biggest challenges of the 21<sup>st</sup> century. Both water and land resources are finite, but demand in various sectors is increasing. Irrigated agriculture, a major contributor in global food production, is one of biggest consumers of fresh water, accounting for about 70% of global diverted water resources. Considering the rapidly growing water demand for

industries and domestic use, it is essential to use irrigation water more efficiently. Most of the large irrigation systems are located in arid to semi-arid regions where rainfall is much less than evaporative demand and agriculture is only possible with surface or groundwater irrigation. As a result, evapotranspiration is one of the largest components in the overall water balance in these regions. Therefore knowledge of actual evapotranspiration in irrigated river basins is essential for efficient management of scarce water resources. Spatial patterns of evapotranspiration explain whether the water is used as “intended” or not.

Conventional methods to compute evapotranspiration are based on climate data (Allen *et al.* 1998). In these methods routinely collected climatic data are used to compute evapotranspiration ( $ET$ ) for a reference crop of alfalfa (Wright and Jensen, 1972) or short uniform grass (Doorenbos and Pruitt, 1977) and then using an area-specific crop coefficient ( $K_c$ ), crop water requirement is calculated for different growth stages of the crop under investigation. Cropped area and  $K_c$  are not known with certainty and general values from the literature are usually used to estimate  $ET$ . Such estimates may differ considerably from the actual evapotranspiration ( $ET_a$ ), due to variations in planting dates, crop growth stages and root-zone moisture conditions. Moreover, conventional techniques provide point estimates and often it is not practically possible to capture all the spatial variation at broad scales such as river basins, which are increasingly recognized as the management unit for irrigation and other water uses.

Actual evapotranspiration can be estimated from satellite remote sensing (Engman and Gurney, 1991; Kustas and Norman, 1996; Bastiaanssen *et al.* 1998 & 2002, Kustas *et al.* 2003). Such methods provide a powerful means to compute actual evapotranspiration from individual pixel to an entire raster image. Emerging developments in the field of remote sensing make it possible to overcome information limitations on soil water status, the actual evaporative depletion and estimation of net groundwater use for agriculture (Scott *et al.* 2003; Ahmad and Bastiaanssen 2003, Ahmad *et al.* 2004). As surface energy balances and crop water stress are directly linked to agricultural water use,  $ET_a$  variations in space and time are thought to be highly indicative for the adequacy and reliability of irrigation as well as the equity in water use. This study demonstrates the application of satellite remote sensing for land use classification and  $ET_a$  estimation in a data scarce basin, the Krishna in India.

High-spatial resolution snapshots of  $ET_a$  using SEBAL derived from Landsat may be usefully supplemented by high temporal resolution satellite imagery such as MODIS. MODIS has been used to map vegetation phenology and cropping pattern in the Krishna Basin (Biggs *et al.*, submitted), and is used to put the Landsat SEBAL results in the context of the annual vegetation and cropping cycles.

## **DESCRIPTION OF THE STUDY AREA**

This research was conducted using Landsat7 ETM satellite imagery of Dec. 29, 2000 covering a part of the Krishna basin, 77°30' to 78°54' E and 16°46' to 18°4' N, in southern India (Figure 1). The Krishna Basin is the fourth largest river basin in India in terms of annual discharge and fifth in terms of basin area. The climate of the basin is predominantly semi-arid. Annual average precipitation is 780 mm and approximately 90% of annual precipitation occurs during the monsoon months of May-October. The Krishna basin has relatively diverse cropping patterns (Neena, 1998). Crops include rice, maize, sorghum, sugarcane, millet, groundnut, and fodder

grass (Pawar, 1989). The area used for the SEBAL analysis has three major cropping regions: a vegetable and cash crop area on black vertisols soils to the west of the city Hyderabad, a wastewater irrigated area downstream of Hyderabad, and tank and groundwater irrigated rice on red alfisol soils to the east and south of Hyderabad. The annual cropping cycle consists of three periods: kharif during the wettest monsoon months (mid June- mid December), rabi in the post-monsoon (mid December-April), and the dry season during the months with little rainfall (mid April-May).

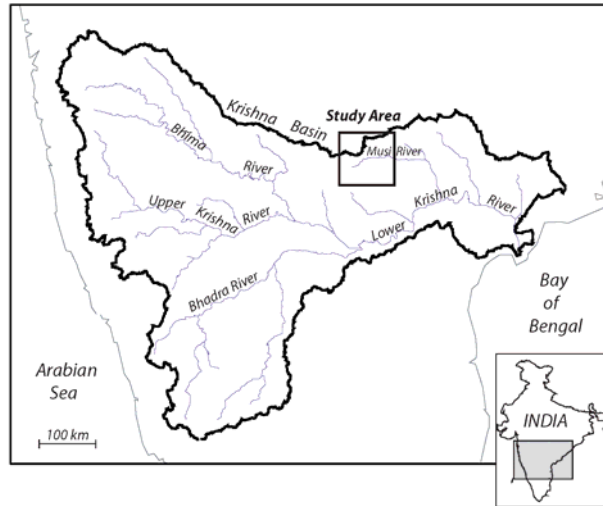


**Figure 1** Location of study area in the Krishna Basin, India.

Weather data on Dec. 29, 2000 are summarized in Table 1, which are obtained from ICRISAT agricultural meteorological station located in the vicinity of Hyderabad, India (Latitude: 17.53° N, Longitude 78.27° E, Altitude: 545 m). Using the Penman-Monteith approach, the reference crop  $ET$  is 3.5 mm per day under these climatic conditions at this location.

**Table 1.** Weather conditions on Dec. 29, 2000 in the Krishna Basin as per record of ICRISAT meteorological station (Latitude: 17.53° N, Longitude 78.27° E).

Max. Temp.	Mini. Temp.	Rel. Humidity %	Rel. Humidity %	Wind Speed	Actual Sunshine	Rain	Pan Evaporation
C°	C°	7.17 hour	14.17 hour	m/sec	Hours	mm	mm
27.4	10.2	90	34	1.44	9.6	0	4.8

## MATERIALS AND METHODS

In this paper, the Surface Energy Balance Algorithm for Land (SEBAL, Bastiaanssen *et al.* 1998) is used to compute  $ET_a$  from satellite imagery having visible, near infrared and thermal infrared bands. SEBAL computes a complete radiation and energy balance along with the resistances for momentum, heat and water vapour transport for each pixel. SEBAL is a well-tested and widely used method to compute  $ET_a$  (Bastiaanssen *et al.* 1998 & 2002, Farah 2001, Tasumi *et al.* 2003, Gieske and Meijninger 2003).

Evaporation is calculated from the instantaneous evaporative fraction,  $A$ , and the daily averaged net radiation,  $R_{n24}$ . The evaporative fraction,  $A$ , is computed from the instantaneous surface energy balance at the moment of satellite overpass on a pixel-by-pixel basis:

$$\lambda E = R_n - (G_0 + H) \quad (1)$$

where  $\lambda E$  is the latent heat flux,  $R_n$  is the net radiation,  $G_0$  is the soil heat flux and  $H$  is the sensible heat flux. The latent heat flux describes the amount of energy consumed to maintain a certain crop evaporation rate. The surface albedo, surface temperature and vegetation index are derived from satellite measurements, and are used together to solve  $R_n$ ,  $G_0$  and  $H$ . The latent heat flux,  $\lambda E$ , is the residual term of the energy budget, and is used to compute the instantaneous evaporative fraction,  $A$ :

$$A = \frac{\lambda E}{\lambda E + H} = \frac{\lambda E}{R_n - G_0} \quad (2)$$

The instantaneous evaporative fraction,  $A$ , expresses the ratio of the actual to the crop evaporative demand when the atmospheric moisture conditions are in equilibrium with the soil moisture conditions. The evaporative fraction tends to be constant during daytime hours; the  $H$  and  $\lambda E$  fluxes, on the contrary, vary considerably. The difference between the instantaneous evaporative fraction at the moment of satellite overpass and the evaporative fraction derived from the 24-hour integrated energy balance is marginal, and may be neglected (Brutsaert and Sugita 1992, Crago 1996, Farah 2001). For time scales of 1 day or longer,  $G_0$  can be ignored and net available energy ( $R_n - G_0$ ) reduces to net radiation ( $R_n$ ). For the daily time scale,  $ET_{24}$  ( $\text{mm d}^{-1}$ ) can be computed as:

$$ET_{24} = \frac{86400 \cdot 10^3}{\lambda \rho_w} A R_{n24} \quad (3)$$

where  $R_{n24}$  ( $\text{W m}^{-2}$ ) is the 24-h averaged net radiation,  $\lambda$  ( $\text{J kg}^{-1}$ ) is the latent heat of vaporization, and  $\rho_w$  ( $\text{kg m}^{-3}$ ) is the density of water.

### Satellite Imagery

The Landsat7 ETM image of Dec. 29, 2000 was obtained from Michigan State University for the study area. For SEBAL analysis, visible, near infrared (NIR) and thermal infrared (TIR) bands are required; the band and sensor characteristics of Landsat7 ETM are presented in table 2.

**Table 2.** Characteristics of Visible and Infrared bands of Landsat7 ETM used for SEBAL application

Satellite Imagery	Spectral Range (microns)	Spatial Resolution (m)
Landsat7 ETM	Band 3: R (0.630-0.690)	30
(8 bit radiometric resolution)	Band 4: NIR (0.750-0.900)	30
	Band 6: TIR (10.400-12.50)	60

Using reflectance (R and NIR) and radiance (TIR) of these images, different surface parameters, NDVI, surface albedo, surface emissivity and surface temperature were derived. Then  $R_n$ ,  $G_0$  and  $H$  are solved using the semi-empirical relationship between these surface parameters. Finally  $ET_a$  is calculated from Eq. 3 for all pixels in the image.

### RESULTS AND DISCUSSION

Using the Dec. 29, 2000 Landsat7 ETM image and routine meteorological data on temperature, humidity, wind speed and sunshine hours, pixel-based daily  $ET_a$  is

computed by solving the surface energy balance using Eq. 1, 2 and 3 for the study area (Figure 2).  $ET_a$  map (Figure 2) clearly indicate spatial patterns of  $ET_a$  for various land use classes that include dry/barren land, native vegetation, agricultural crops and water bodies. The computed  $ET_a$  ranged from 0 to 4.7 mm per day. The highest value of  $ET_a$  is observed for water bodies and is in the same range as pan evaporation measured at the meteorological station located within the image (See Table 1).

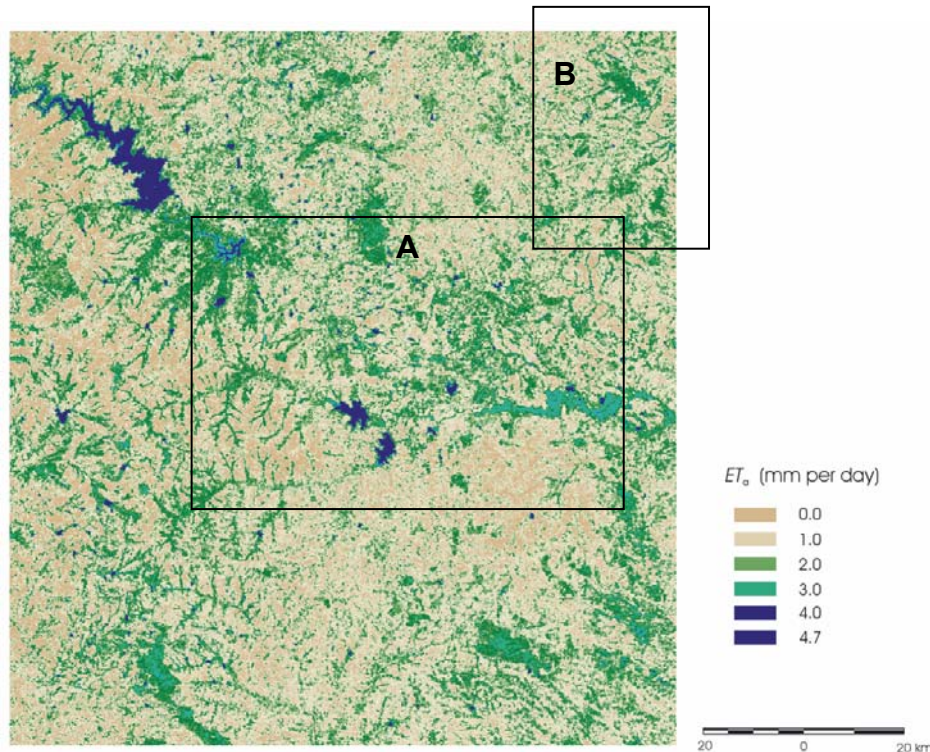


**Figure 2.** Actual Evapotranspiration  $ET_a$  estimates using SEBAL for Landsat7 ETM imagery for Krishna Basin. Dec. 29, 2000. A and B correspond to areas selected for detailed comparison presented in Table 3.

There are large tracts of rocky/barren land with almost zero evaporation. Dry grasslands on black soils have the lowest  $ET_a$ . Some bare rocks occur in the scene, but these tend to be rather small (10-50m diameter) and are surrounded by shrubs with relatively high  $ET_a$ , giving the rocky-shrub lands a higher  $ET_a$  than the grasslands. The average value of  $ET_a$  for the whole image is 1.6 mm per day. Irrigated fodder grass along the head reach of the Musi River, with no apparent water stress, evaporates at a maximum rate of 3.4-3.5 mm per day, almost the same as Penman-Monteith reference crop  $ET_0$ . This indicates that estimated values of  $ET_a$  from SEBAL are in good agreement with local field measurements for wet land surfaces.

To investigate inter- and intra  $ET_a$  variations for different land use classes in the Krishna Basin,  $ET_a$  statistics (Table 3) from 12 different land uses were calculated using 44 representative polygons delineated using data from field surveys and visual image interpretation (Figure 3). This allowed separation of land use types that were not easily separated in an image classification due to mixed spectral information and different sources of irrigation, including riparian vegetation versus irrigated paragrass, groundwater irrigated versus wastewater irrigated areas, and plantations versus natural deciduous forest). For example, “natural vegetation” may include a mixture of rock,

bare soil, and vegetation with different phenologies, a groundwater irrigated corridor contains a mosaic of different crops in different stages of growth, and the irrigated fodder paragrass corridor includes all rotations of the 30-day harvest cycle.

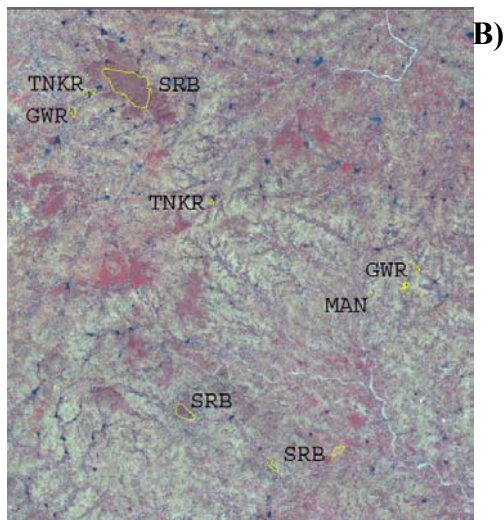
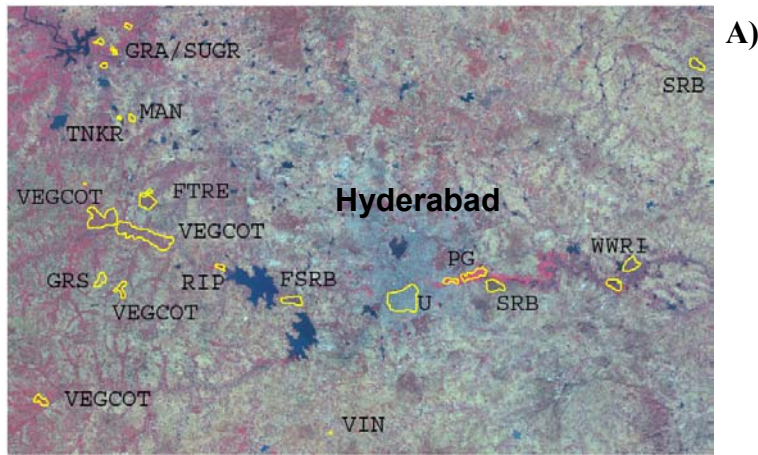


**Figure 3.** Landsat image showing polygons used to determine  $ET_a$  for representative land cover types. See Table 3 for names. A and B correspond to the frames in Figure 2.

**Table 3.**  $ET_a$  variation for dominant land use pattern in Krishna Basin.

Name	Map code	Stage of growth	Mean mm/day	St Dev	Coef of variation
Water bodies		-	4.45	0.21	0.05
Irrigated fodder paragrass	PG	Rotational	3.16	0.23	0.07
Wastewater irrigated rice	WWRI	Begin second crop	3.32	0.24	0.07
Tank irrigated rice	TNKR	Between crops	2.66	0.44	0.17
Groundwater irrigated rice	GWR	Between crops	2.62	0.37	0.14
Vegetables and cotton	VEGCOT	End first crop	2.20	0.49	0.22
Rainfed grains	GRA	End first crop	2.50	0.26	0.10
Fruit plantations	MAN, VIN	End major crop	1.87	0.36	0.19
Forest (tree dominant)	FTRE	Mid-senescence	2.69	0.40	0.15
Shrubs-grassland	FSRB, SRB	Mid-senescence	2.52	0.36	0.14
Grassland	GRS	Mid-senescence	0.74	0.35	0.47
Urban	U	-	1.35	0.44	0.32

The wastewater irrigated area, including both paragrass and rice, has the highest  $ET_a$  in the image. Rice irrigated near tanks and by groundwater wells show  $ET_a$  values that are lower by 0.7 mm per day (20%). Rainfed crops have nearly the same  $ET_a$  as light-irrigated vegetable and cash crops (cotton). Plantations, mostly mangos, have the lowest  $ET_a$  of all crops at 1.9 mm per day. Grasslands have the lowest  $ET_a$  in the image, less than 50% of the next-lowest class. This is likely due to the shallow rooting depth of grass relative to the other vegetation types in the image.

The low  $ET_a$  from plantations reflects the large spacing and low LAI of plantations relative to forests and green shrubs. Mango plantations have a field-estimated canopy cover of 15-25%, with bare soil between trees. Forests and shrubs tend to have higher canopy coverage and understory vegetation.

The interpretation of the  $ET_a$  values depends critically on understanding vegetation phenology and cropping cycle at the time of image acquisition. The 8-day MODIS time-series of NDVI from May 2000-May 2001 shows the December 29, 2000 image in the context of the annual vegetation cycle for irrigated crops (Figure 4a) and rainfed areas (Figure 4b). The December 29 image occurs at the end of the monsoon growing season for rainfed agriculture, rainfed ecosystems and groundwater irrigated systems, and at the beginning of the second cropping season for the wastewater irrigated area. Wastewater irrigated paragrass has perennially high NDVI that fluctuates relatively little due to the constant rotation of small patches on a 30-day cycle. The December image occurs between the monsoon and post-monsoon crops of groundwater/tank irrigated rice, when NDVI is at a seasonal low and land cover is a mix of low stubble from recently harvested area, and flooded area in newly planted paddy. The wastewater irrigated area, by contrast, has an earlier onset of cropping and is in the middle of the development phase of the crop. Vegetative cover consists of 10-40 cm tall rice plants. Supplemental irrigated vegetable-cotton cropping is in the harvest and senescence phases.

The  $ET_a$  differences are related to both irrigation and vegetation phenology. Wastewater irrigated rice has the highest  $ET_a$  of the image since it is a relatively homogenous cover of growing crop in the middle of its growth stage. The  $ET_a$  from paragrass is somewhat lower due to the rotational harvesting which results in a mosaic of grass in different stages of growth.  $ET_a$  from groundwater irrigated rice is lower than  $ET_a$  from wastewater irrigated rice. Both (crop growth stage and deficit irrigation) might cause the low SEBAL  $ET_a$  in GW rice, but it's difficult to disentangle without some field confirmation and/or longer time series analysis. Similarly, vegetable-cash-rainfed cropping has a lower  $ET_a$  compared with wastewater irrigated rice partly because the image occurs during the harvest and senescence phases of the cropping cycle. Interestingly, the grassland, which has the lowest  $ET_a$  of all classes in December, has nearly the same NDVI as shrubland and forest during the monsoon, suggesting that its low  $ET_a$  is mostly due to its rapid senescence at the end of the monsoon season.

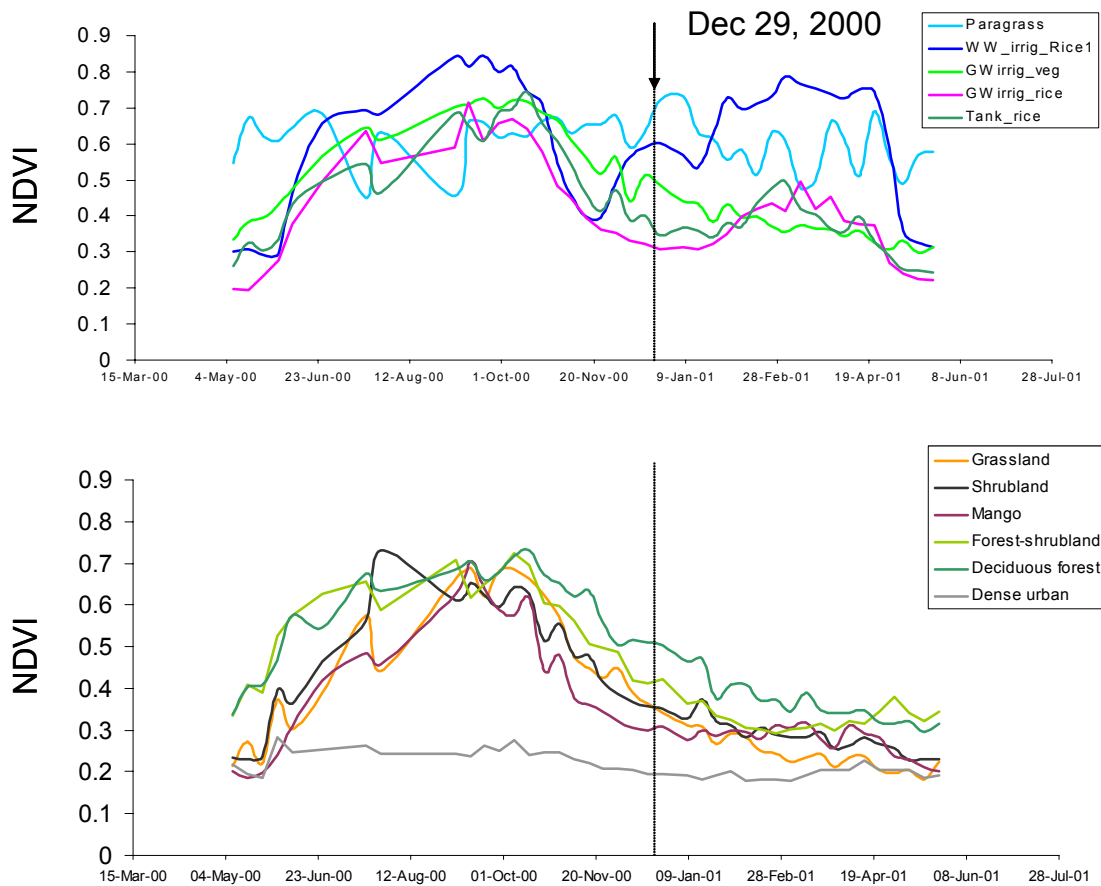


**Figure 4.** NDVI variation for different land use classes in Krishna Basin. (Based on 8-day MODIS time-series of NDVI from May 2000-May 2001)

### SUMMARY AND CONCLUSIONS

The purpose of this study was to demonstrate the application/utility of the SEBAL technique to map spatial variation in actual evapotranspiration for the data-scarce Krishna River basin. Data requirements for SEBAL processing include any satellite imagery with visible, near-infrared and thermal-infrared band such as Landsat, NOAA AVHRR, MODIS and ASTER and routine meteorological measurement of air temperature, humidity, wind speed and sunshine duration. In this study a Landsat7 image of Dec. 29, 2000 was used to solve net radiation, soil heat flux and sensible heat flux components of the energy balance. Latent heat flux, the residual term of surface energy balance (Eq. 1), was used to compute evapotranspiration for every 30m\*30m pixel. Another advantage of the SEBAL approach over conventional  $ET$  estimation methods is that it does not require detailed field information such as crop or land use type, sowing date, moisture status or area specific crop coefficients  $K_c$ , which are essential to compute  $ET$  using conventional techniques. However, critical to the interpretation of the SEBAL results is knowledge of cropping calendars; many of the differences between land cover types were due to differences in vegetation phenology, so the snapshot SEBAL results may not be representative of annual  $ET_a$ . A full time series of SEBAL would be needed to evaluate seasonal differences in  $ET_a$  from different vegetation types. The current snapshot demonstrates that shrublands and forests have  $ET_a$  comparable to the  $ET_a$  from rainfed and supplemental irrigated areas. Grasslands have very low  $ET_a$  as early as December, less than 2-3 months

following the end of the monsoon, likely due to their shallow rooting depth relative to other vegetation types.

The combination of red, near infrared, and thermal infrared Landsat bands, which are used to calculate the surface energy balance and actual evapotranspiration from latent heat flux, and MODIS-derived land cover allow interpretation of the adequacy of irrigation. The study results indicate that perennially irrigated fodder grass and seasonal rice under wastewater irrigation downstream of a major urban center have the highest  $ET_a$ . Groundwater and tank-irrigated rice, although at a different crop growth stage on the 29 Dec. 2000 date of image acquisition, have lower evapotranspiration, suggesting reduced irrigation adequacy as corroborated by field experience. Given the lack of data on irrigation applications under any of the three principal sources of water—wastewater, groundwater, tanks—in the image, the remote sensing tools applied here offer considerable advantage over time-consuming conventional  $ET_a$  estimation methods. However, interpretation of the results is greatly strengthened through field-based observations.

## REFERENCES

- Ahmad, M.D., W.G.M. Bastiaanssen, and R.A. Feddes, 2004. A new technique to estimate net groundwater use across large irrigated areas by combining remote sensing and water balance approaches. *Hydrogeology Journal* [<http://www.springerlink.com/index/10.1007/s10040-004-0394-5>]
- Ahmad, M.D. and W.G.M. Bastiaanssen, 2003. Retrieving soil moisture storage in the unsaturated zone using satellite imagery and bi-annual phreatic surface fluctuations. *Irrigation and Drainage Systems*. 17(3): 141-161.
- Allen, R. G., L. S. Pereira, D. Raes, and M. Smith, 1998. Crop evapotranspiration, guidelines for computing crop water requirements, FAO Irrig. and Drain. Pap. 56, 300 pp., Food and Agric. Organ. of the U. N. (FAO), Rome, Italy.
- Bastiaanssen, W. G. M., Ahmad, M. D., and Chemin, Y., 2002. Satellite surveillance of evaporative depletion across the Indus. *Water Resources Research* 38(12): 1273, 1-9.
- Bastiaanssen, W.G.M., M. Menenti, R.A. Feddes and A.A.M. Holtslag, 1998. A remote sensing surface energy balance algorithm for land (SEBAL), part 1: formulation, *Journal of Hydrology*. 212-213: 198-212.
- Biggs, T. W., P. S. Thenkabail, M. K. Gumma, C. Scott, G. R. Parthasaradhi, and H. Turrall. submitted. Vegetation phenology and irrigated area mapping using MODIS time-series, ground surveys, and agricultural census data in Krishna River Basin, India. *International Journal of Remote Sensing*.
- Brutsaert, W. and M. Sugita, 1992. Application of self-preservation in the diurnal evolution of the surface energy budget to determine daily evaporation. *J. of Geophysical Res.*, 97, D17: 18,322-18,377.
- Crago, R.D. 1996. Conservation and variability of the evaporative fraction during the day time. *J. Hydrol.* 180: 173-194.
- Doorenbos, J. and W.O. Pruitt, 1977, Crop water requirements. *Irrigation and Drainage Paper no. 24 (revised)*, FAO, Italy, 144pp.

- Engman, E.T., and R.J. Gurney, 1991. Remote sensing in hydrology; Chapman and Hall, London.
- Farah, H.O., 2001. Estimation of regional evaporation using a detailed agro-hydrological model. *J. of Hydr.* 229(1-2): 50-58.
- Gieske, A. and W. Meijninger 2003. High density NOAA time series of ET in the Gediz Basin, Turkey, . ICID Workshop on Remote Sensing of ET for Large Regions, Montpellier, France 17 Sept. 2003.
- Kustas WP, GR Diak and MS Moran 2003. Evapotranspiration, Remote Sensing of. *Encyclopedia of Water Science* pp 267 – 274. Marcel Dekker, Inc., New York.
- Kustas, W.P. and J.M. Norman, 1996. Use of remote sensing for evapotranspiration monitoring over land surfaces; *Hydr. Sci. J.* 41(4): 495-516.
- Neena, D. 1998. Inter-state variation in cropping pattern in India. *Indian Journal of Regional Science* 30:57-69.
- Pawar, C. T. 1989. Impact of Irrigation: A regional perspective. Himalaya Publishing House, Bombay.
- Scott, C.A., W.G.M. Bastiaanssen, and M.D. Ahmad, 2003. Mapping root zone soil moisture using remotely sensed Optical Imagery. *Journal of Irrigation and Drainage Engineering ASCE* 129(5): 326-335.
- Tasumi,M., R. Trezza, R. G. Allen and J.L. Wright 2003, U.S. Validation tests on the SEBAL model for evapotranspiration via satellite. ICID Workshop on Remote Sensing of ET for Large Regions Montpellier, France 17 Sept. 2003.
- Wright J.L., and M.E. Jensen, 1972. Peak water requirements of crops in Southern Idaho. *J. Irrig and Drain Div., ASCE* 96(1), 193-201.